Structural characterization of Sol-Gel derived Sr-substituted calcium phosphates with anti-osteoporotic and anti-inflammatory properties.

Guillaume Renaudin, Patrice Laquerriere, Yaroslav Fillinchuk, Edouard Jallot, Jean-Marie Nedelec

Structural characterization of Sol-Gel derived Sr-substituted calcium phosphates with anti-osteoporotic and anti-inflammatory properties.

G. Renaudin[1], P. Laquerrière[2], Y. Filinchuk[3], E. Jallot[4] and J.M. Nedelec[1*]

[1] Laboratoire des Matériaux Inorganiques CNRS UMR 6002. Université Blaise Pascal & Ecole Nationale Supérieure de Chimie de Clermont-Ferrand - 24 avenue des Landais, 63177 Aubière Cedex, France.

[2] INSERM, U 926, IFR 53, 1 rue du Maréchal Juin, BP 138, 51095 Reims, Cedex, France.

[3] Swiss-Norwegian Beam Lines at ESRF, 6 rue Jules Horowitz, BP 220, 38043 Grenoble, France

[4] Laboratoire de Physique Corpusculaire de Clermont-Ferrand CNRS/IN2P3 UMR 6533. Université Blaise Pascal - 24 avenue des Landais, 63177 Aubière Cedex, France.

[*]Corresponding author : J.M. Nedelec
Laboratoire des Matériaux Inorganiques CNRS UMR 6002, Université Blaise Pascal and ENSCCF
j-marie.nedelec@univ-bpclermont.fr + 33 4 73 40 71 95

Abstract

Sol-Gel chemistry has been successfully used to prepare un-doped and Sr-doped calcium phosphate ceramics exhibiting a porous structure. The samples composition is very close to the nominal one. All samples present phase mixtures mainly Hydroxyapatite (HAp) and Tri Calcium Phosphate (β-TCP). Doping with Sr^{2+} ions has a clear effect on the proportions of the different phases, increasing the amount of β-TCP. An amorphous phase is also observed incorporating some 40 % of the total amount of strontium. Strontium ions also substitute for calcium both in HAp and β-TCP in specific sites that have been determined from Rietveld refinement on synchrotron powder diffraction data. The soluble amorphous and TCP phases are responsible for a beneficial partial release of strontium ions in solution during interactions between the material and biological fluids. Preliminary *in vitro* study demonstrates anti-inflammatory effect of strontium for human monocytes cultured in contact with calcium phosphates.

1. Introduction

Due to the global aging of the population, the need for bone substitutes is increasing very quickly. There is also a strong demand for bioceramics with specific properties such as anti-inflammatory, bactericidal or anti osteoporotic. Bone mineral mass is dominated by nano-crystalline non-stoichiometric hydroxyapatite (Hap, $Ca_5(PO_4)_3OH$) and whitlockite (β-TCP, β-$Ca_3(PO_4)_2$) can be found at many different sites in the human body [1-3]. For these reasons, apatite and whitlockite have been widely used as biocompatible materials for bone replacement and for bone protheses coating [4]. An interesting alternative is the use of so called Biphasic Calcium Phosphate (BCP) which is mixture of HAp and β-TCP. Because of the difference in the solubility of the two phases, the solution behaviour of BCP can be easily tuned. Another interesting possibility is to perform ionic substitution in calcium phosphates to improve their properties and to modulate their bioactivity.

Similarly to the case of Ca, an estimated 99% of the total amount of Sr in the body is confined in bone [1]. The total amount of Sr in human skeleton is small but not insignificant; the Sr/Ca ratio is in the range 0.1-0.3 weight ‰ [5]. Sr is readily taken up in bone [6]. Various studies investigating the therapeutical and detrimental effects of Sr have been carried out on animals and humans [1, 7-12]. *In vitro* and *in vivo* studies have indicated that oral strontium intake not only increases bone formation, the number of bone-forming sites and the bone mineral

density, but also reduces bone resorption [1,10-12]. Sr is used for treatment of osteoporosis [13,14], and was found to induce osteoblast activity when introduced in biocompatible bone cements [15-19]. A better osteointegration has been observed when Sr is present at low concentration level in biomaterials. The role of strontium in human pathology has attracted less attention than the other two important alkaline earths calcium and magnesium. However there has been an increasing awareness of the potential biological role of strontium and its incorporation in calcium phosphate cements has been largely studied in the last decade [15,16,20-30]. The purpose of this study was to examine the incorporation of Sr^{2+} ions in hydroxyapatite sample at the atomic level: identification and quantification of the crystallised phases, identification of the Sr-occupied crystallographic sites, identification of an amorphous phase and determination of the chemical composition of the different phases.

2. Experimental

2.1 Sol-Gel elaboration of Sr-substituted hydroxyapatite

The sol-gel route previously proposed by the authors [31, 32] has been used. Briefly, to produce 2 g of pure HAp powder, 4.7 g of $Ca(NO_3)_2{\cdot}4H_2O$ (Aldrich), 0.84 g of P_2O_5 (Avocado Research chemicals) were dissolved in ethanol under stirring and refluxed at 85°C during 24 h. Then, this solution was kept at 55°C during 24 h, to obtain a white consistent gel and further heated at 80°C during 10 h to obtain a white powder. Finally, the powder was heated at 1100°C during 15 h. To prepare Sr-substituted hydroxyapatite, the required amount of $Sr(NO_3)_2$ (Aldrich) was added to the solution.

Two samples have been studied: pure hydroxyapatite sample (named ‘HAp’ in this paper) of nominal composition $Ca_5(PO_4)_3{\cdot}OH$ and 5% Sr-doped hydroxyapatite sample: named ‘Sr:HAp’ in the following. The doped sample corresponds to an hydroxyapatite where 5 atomic % of calcium have been replaced by strontium atoms thus achieving the nominal composition $Ca_{4.75}Sr_{0.25}(PO_4)_3{\cdot}OH$.

The chemical composition of the hydroxyapatite powders were determined by ICP-AES (Inductively Coupled Plasma-Atomic Emission Spectrometry). The nominal and experimental compositions of the two HAp samples are listed in Table 1. As usually observed for sol-gel derived ceramics [33], the nominal compositions have been readily achieved.

2.2 Characterization of HAp samples

Scanning Electron Microscopy Analysis

The hydroxyapatite powders were deposited on carbon disks and sputter-coated with 20 nm of gold. Then, the samples were examined using a JEOL JSM-5910 LV scanning electron microscope at an accelerating voltage of 15 kV. All the images were recorded using the secondary electrons detector. A representative SEM image is shown in Figure 1 demonstrating the porosity of sol-gel derived HAp samples.

[Figure 1 around here]

Specific Surface Area(SSA) measurements

SSAs were calculated with the BET model from the adsorption isotherm measured by nitrogen sorption analyses at 77 K using an Autosorb MP1 Quantachrome equipment. SSAs are found to be equivalent for both samples around 0.5 $m^2.g^{-1}$. These values were considered for *in vitro* release studies keeping a constant surface/volume ratio.

In vitro Sr^{2+} release studies

The interactions between the ceramics and a biological medium have been carried out at 37°C for 1 to 6 days by immersing about 10 mg of powder in a standard Dulbecco's Modified Eagle Medium (DMEM), which composition is almost identical to the one of human plasma. The specific surface area to DMEM volume ratio was fixed at 500 cm^{-1}. These *in vitro* assays were conducted under static conditions: biological fluids were not renewed and therefore contained only limited amount of P and Ca. Namely, this is a good approach for further development and to compare different doping elements and compositions. ICP-AES was used to analyze the biological fluid before and after bioceramics interactions.

2.3 X-rays powder diffraction

Synchrotron measurement

Synchrotron powder diffraction data of both samples were obtained at ESRF (Grenoble, France) on the SNBL. Finelly grinded powders were introduced into a 0.3 mm diameter glass capillary. Data collections were performed at 295 K with a MAR345 Image Plate detector by using a monochromatic wavelength of λ = 0.710130 Å. The calculated absorption coefficient was $m\mu R = 0.68$ (m = powder packing factor and μ = linear absorption coefficient, R = radius of the capillary, 0.15 mm). Two sample-to-detector distances were used (150 and 350 mm) in

order to combine the benefits of a high resolution and an extended 2θ range. The detector and the wavelength were calibrated with NIST LaB_6. The highest resolution of the MAR345 detector was used: 3450 x 3450 pixels with a pixel size of 100 μm. The exposure time was 60 seconds with a rotation of the capillary by 60°. The two-dimentionnal data were intergreted with Fit2D program [34] which produced correct intensity in relative scale. This 2D detector was used in order to perfectly define the background line, to observe very weak diffraction peaks, and to improve an accuracy of the integrated intensities by achieving a better powder average. Uncertainties of the integrated intensities were calculated at each 2θ-point applying Poisson statistics to the intensity data, considering the geometry of the detector. The Instrument Resolutions Functions were determined from the LaB_6 data.

Rietveld refinements

Joint Rietveld refinements based on the simultaneous use of the data measured at 150 mm (large two theta interval) and 350 mm (high resolution) sample to detector distances were performed for both samples with the program Fullprof.2k Multi-Pattern [35]. Three phases have been refined for the HAp sample: hydroxyapatite, whitlockite and lime. For the Sr:HAp sample, portlandite has been introduced as the fourth phase. The absence of calcite in both samples has been verified. The structural parameters of hydroxyapatite, $Ca_5(PO_4)_3{\cdot}OH$, were taken from [36]: space group $P6_3/m$, Z = 2, a = 9.4218 Å and c = 6.8813 Å, 7 independent atomic positions: two Ca, one P and four O positions. The O4 oxygen position (*i.e.* the hydroxyl anion) is half occupied, this corresponds to a statistically disordered 4*e* position around the 2*a* (0,0,¼) site. The structural parameters of whitlockite, β-$Ca_3(PO_4)_2$, were taken from [37]: space group $R3c$, Z = 21, a = 10.4352 Å and c = 37.4029 Å, 18 independent atomic positions: five Ca, three P positions and ten O positions. The structural parameters of lime, CaO, were taken from [38]: space group $Fm\bar{3}m$, Z = 4, a = 4.8071 Å. And the structural parameters of portlandite, $Ca(OH)_2$, were taken from [39]: space group $P\bar{3}m1$, Z = 1, a = 3.589 Å and c = 4.911 Å. In a first step all the structural parameters were fixed according to the literature values. Then during the successive refinement cycles they were all refined (first lattice parameters and peak profiles, and next atomic parameters: positional, isotropic temperature and occupancy factors). In the final run, 96 and 115 parameters were refined for the HAp sample (2 zero shifts, 6 scale factors, 20 profil parameters and 68 structural parameters) and for the Sr:HAp sample (2 zero shifts, 8 scale factors, 28 profil parameters and 77 structural parameters) respectively. The determination of the Instrumental Resolution

Function (extracted from the powder patterns recorded on NIST LaB_6 powder) improved the peak profile modelling while decreasing the number of profile parameters. It allowed also the extraction of the sample intrinsic microstructural parameters: average apparent crystallite size and average maximum strain. The diffraction profiles (both instrumental and sample intrinsic) were modelled by using a Thomson-Cox-Hastings pseudo-Voigt function [35]. Refinement with the anisotropic line broadening procedure [35] did not improve significantly the fit. Correction applied by taking into account microabsorption effect, as indicated by [40], did not affect the quantitative Rietveld analysis result (due to a nearly equivalent linear absorption coefficient for all the phases). The use of the monoclinic ordered structural description for the hydroxyapatite phase [41] did not allow increasing the accuracy of the refinement. The last refinement cycles were performed by introducing hydrogen atom from hydroxyl anion. The H4 position was located the site 4*e* (in accordance with [37]), a soft constraint of 0.92 ± 0.05 Å was applied to the distance O4-H4, and the isotropic temperature factors of H4 was constrained to be 1.2 times B_{iso} of the corresponding oxygen atom O4 as it is usual for hydroxyl groups [42]. The final refined $d_{O4\text{-}H4}$ distances were 0.89(2) Å and 0.92(2) Å for respectively the pure and the Sr-doped hydroxyapatite phase. Previously unconstrained distance converged to 0.67(7) Å in the case of the pure hydroxyapatite phase, and did not converge in the case of the Sr-doped hydroxyapatite phase. The refined structural parameters for hydroxyapatite and whitlockite phases are respectively summarized in Table 2 and Table 3. Rietveld plots are shown in Figures 2 and 3 for HAp and Sr:HAp samples, respectively.

[Tables 2 and 3 around here]

[Figures 2 and 3 around here]

2.4 Preliminary biological study of inflammation reactions

Cell culture

Elutriated monocytes were used to evaluate Tumor Necrosis Factor (TNF-α) production. Monocytes from five healthy consenting donors were collected by leukapheresis and purified by counterflow elutriation. Purity, after CD14 staining, was at least 95%, the rest being neutrophils. Cells were maintained in RPMI-1640 medium (Life Technologies, France) supplemented with 10% fetal calf serum (Life Technologies, France), 2 mM glutamine, penicillin (5000 $U.mL^{-1}$, Life Technologies) and streptomycin (25 $\mu g.mL^{-1}$, Life

Technologies) at 37°C in a saturated 5% CO_2 - 95% air atmosphere. All reagents were certified endotoxin-free. The cells were cultured in petri dishes (Life Technologies). The density was 2.10^5 cells.mL^{-1} in a 5 mL total volume. Cells of each donor were exposed during 6h (time chosen to have an interaction between cells and particles) to the different particles described above. The negative control consisted of monocytes in culture medium alone (data not shown) and the positive control was monocytes plus LipoPolySaccharide (LPS). LPS (Sigma-Aldrich) were chosen because of their inflammatory actions on the target cells.
The viability of cells was evaluated by trypan blue exclusion test. The viability was >95% in all of the experiments (before and after exposure to particles).

Quantification of TNF-α by ELISA

After 6h, TNF-α determinations in cell culture supernatants were performed using commercially available ELISA kits (Quantikine, R&D Systems, Inc., Minneapolis, MN) according to the manufacturer's instructions. The sensitivity of each kit was 7.8 pg.mL^{-1}. Results are presented in relative concentration. Results were presented as median ± interquartile space (IQS) of relative variation between positive control and stimulated cells.
A Mann & Whitney non parametric test was performed to compare the different conditions.

3. Results and discussion

3.1 Quantitative phases analysis

Quantitative phases analysis has been performed on the basis of the joint Rietveld refinements. Three phases have been observed and quantified in case of HAp sample (apatite, whitlockite and lime). Portlandite has been introduced as the fourth phase in Sr:HAp sample. Results of the quantitative phase analysis are summarized in Table 4.

[Table 4 around here]

Synthesis conditions correspond to hydroxyapatite single phase samples; *i.e.* a (Ca+Sr)/PO_4 ratio of 1.67. However both syntheses yielded multiphase samples. The HAp sample contained 93 wt % of apatite but only 65 % for Sr-HAp. The presence of whitlockite, with a lower Ca/PO_4 ratio of 1.50 was compensated by the presence of CaO. Nevertheless a deficit in alkaline earth atoms was observed: it is in the range of the standard deviation in the case of HAp sample, and more pronounced in the case of Sr:HAp sample (*i.e.* respectively 1.66(2) and 1.63(3) refined ratios). This deficit in the case of Sr:HAp sample has to be explained by

the presence of an alkaline-earth rich amorphous phase, not accessible by X-ray diffraction. This amorphous phase can be expressed as an amorphous (Ca,Sr)O equivalent. According to the apparent Sr deficit in the crystallised phases (indicated by the refined compositions of $Ca_{4.88(1)}Sr_{0.12(1)}(PO_4)_3(OH)$ and $Ca_{2.87(6)}Sr_{0.13(6)}(PO_4)_2$ leading to a Sr amount of only 2.86(4) %) the amorphous (Ca,Sr)O should mainly be composed of strontium oxide. Calculation has been performed, in the case of Sr:HAp sample, to estimate the amount of amorphous phase by simultaneous comparison of the nominal and refined $(Ca+Sr)/PO_4$ ratios and the nominal and refined Sr amounts (see Table 4). An estimation of 2.2 wt % of amorphous (Ca,Sr)O, which in composed at around 90 wt % by strontium oxide, was obtained. These results indicates that a large amount of about 40 % of the Sr introduced during the synthesis is present in the amorphous phase, about 32 % is inserted in the apatite phase (of composition $Ca_{4.88(1)}Sr_{0.12(1)}(PO_4)_3{\cdot}OH$, relatively far from the theoretical $Ca_{4.75}Sr_{0.25}(PO_4)_3{\cdot}OH$ composition corresponding to the synthesis of a single phase Sr:HAp sample) and about 28 % is inserted in the whitlockite phase (with the $Ca_{2.87(6)}Sr_{0.13(6)}(PO_4)_2$ composition). Rietveld refinement for the HAp sample indicated that a very small amount of CaO (*i.e.* 0.2 wt %) led to the formation of a noticeable amount of whitlockite (*i.e.* 7.0 wt %) due to the close Ca/PO_4 ratio between hydroxyapatite (1.67) and whitlockite (1.50) phases. Introduction of strontium during the synthesis increased the formation of the alkaline earth oxide with a poorly crystalline feature (from 0.2 wt % in HAp sample to about 3 wt % in Sr:HAp sample by considering lime, portlandite and the amorphous equivalent) which is likely located at the surface of the crystallised grains of hydroxyapatite and withlockite in the form of thin amorphous surface layer). The appearance of whitlockite in the Sr containing apatite samples has been previously reported [22, 24, 43]. Nevertheless the presence of a small amount (less than 1 wt % evaluated from high quality X-ray powder patterns) of CaO, as well as $Ca(OH)_2$ and the amorphous equivalent, simultaneously with the whitlockite phase indicated that the whitlockite formation is not attributed to the non-stoichiometry of the apatite structure. At high temperature, the Sr-doped whitlockite phase is more stable than the Sr-doped hydroxyapatite phase and its formation is compensated by the combined extraction of alkaline earth oxide in order to keep the ratio $(Ca+Sr)/PO_4 = 1.67$. This observation correlates with the fact that single phase poorly crystalline Sr-HAp samples are obtained by a moderate heat treatment [20,28]. Such a hydroxyapatite inhibiting formation, favouring whitlockite formation has already been described in the case of smaller Mg^{2+} ions insertion [44].

3.2 Sr-hydroxyapatite solid solution study

This study investigated to Ca-rich side of the Sr-apatite solid solution, *i.e.* $Ca_{5-x}Sr_x(PO_4)_3{\cdot}OH$ with x = 0 and 0.12. The solid solution extends from x = 0 (*i.e.* undoped hydroxyapatite) to x = 5 (*i.e.* belovite $Sr_5(PO_4)_3(OH)$ [46]). Figure 4 reports the lattice parameters and unit cell volume variations in the solid solution according to the present study and from the literature for x = 0 [34], 0.09 [46], 0.51 [47], 1.158 [47], 3.192 [47] and 5 [45]. The compound with x = 0.09 [46] has to be carefully considered here because of its non stoechiometric hydroxyl amount as indicated by its composition $Ca_{4.71}Sr_{0.09}H_{0.2}(PO_4)_3(OH)_{0.80}$. Lattice parameters indicated in [28] for x = 0, 0.003, 0.015 and 0.15 (*i.e.* *a* = 9.3689, 9.3825, 9.3997 and 9.4252 Å respectively, and *c* = 6.8798, 6.8929, 6.9060 and 6.9591 Å respectively) are not considered here as they differ significantly from the other values.

[Figure 4 around here]

The variation of the unit cell as a function of the x value follows a linear Vegard's law. A careful examination of these dependences at the Ca-rich side revealed a slight deviation from the linear Vegard's law for both *a* and *c* lattice parameters, and consequently for the unit cell volume (see insets in Figure 4). This observation should be correlated with the preferential insertion of strontium atoms in the 6*h* site; *i.e.* the site Ca2 connected to the disordered O4 position of the hydroxyl anion (see Figure 5).

[Figure 5 around here]

The statistical occupancy disorder of this O4 position corresponds to a shift from the special 2*a* position (0,0,¼). This O4 site is the only oxygen position that do not belong to a rigid phosphate $[PO_4]^{3-}$ tetrahedra. An increase of the O4 shift from the special 2*a* site can locally accommodate the replacement of calcium atoms by bigger strontium atoms. The displacement of O4 position from (0,0,0.2030) to (0,0,0.191) allowed to increase the Ca2-O4 distances (represented with broken bonds in Figure 5b) from 2.38 Å in the pure hydroxyapatite phase to 2.40 Å in the Sr-doped hydroxyapatite phase. Rietveld refinement results provide an evidence for strontium being located only in the Ca2 site in our low Sr-substituted hydroxyapatite (x = 0.12). In the same way, Bigi *et al.* found a preferential substitution of Sr in this Ca2 position for x = 0.51, 1.158 and 3.192 [47] (*i.e.* the occupancy factor for Sr2 position in the 6*h* site was systematically higher than the occupancy factor of Sr1 position in the 4*f* site). The case with x = 0.09 disagrees with this observation, but as already mentioned this compound behaves

differently due to its low hydroxyl content [46]. The displacement of the hydroxyl groups along the *z* axis, at low substitution level, accommodates the insertion of Sr atoms in the hydroxyapatite structure with a moderate influence on the lattice parameters (*i.e.* explaining the deviation from the linear Vegard's law at the Ca-rich side of the solid solution).

3.3 Sr-doped whitlockite study

This study investigated the insertion of small amount of Sr in the whitlockite structure. Table 3 indicates that Sr is preferentially inserted in the site Ca4. More generally Sr was inserted in the low density column described and named by Yashima et al. the A column [37] (see Figure 2 in [37]). 75 % of inserted Sr atoms are located in this A column (composed of the sites Ca4 and Ca5), compared to only 25 % of inserted Sr atoms in the dense B column (made of the Ca1, Ca2 and Ca3 sites). Figure 6 represents the five independent Ca sites in Sr-free whitlockite. The Ca4 site presents an unusually low coordination number (CN = 3) with a planar polyhedron in pure whitlockite [37]. If we take into account the three following neighbouring oxygen atoms, a coordination number of 6 can be assumed, with three shorter $d_{Ca4\text{-}O1}$ = 2.53 Å and three larger distances $d_{Ca4\text{-}O9}$ = 3.12 Å (the latter are represented by broken lines in Figure 6d). Although such coordination polyhedron is more appropriate, a deficiency in the calculated bond valence [48] remains for Ca4: the bond valence sum (BVS) equals 0.68 or 0.79 by taking into account 3 or 6 neighbouring oxygens respectively. In our sample, the half-occupied Ca4 site is 25 % - 25 % occupied by Ca and Sr atoms. This large insertion of strontium in the Ca4 site modifies its coordination polyhedron. In the Sr-doped whitlockite structure, the Ca4 site has six neighbouring oxygen atoms with quite equivalent (Ca, Sr)-O bond distances: three distances $d_{Ca4\text{-}O1}$ = 2.63 Å and three distances $d_{Ca4\text{-}O9}$ = 2.79 Å. These six bonds give the calculated BVS of 1.03 (by considering Ca4 occupied by 25 % Ca and 25 % Sr) which is still too low for a divalent cation. The insertion of Sr in the Ca4 site has clearly a stabilising effect on the whitlockite structure. Not only the geometrical shape of the Ca4 polyhedron is considerably improved, but also those for the other cation sites. Figure 6 represents the environments of all the cationic sites as refined in the Sr-doped whitlockite. Ca1, Ca2 and Ca3 compose the dense B column [37] and have CN = 8 with a more or less distorted monocapped pentagonal bipyramidal coordination polyhedra. The stabilising effect of Sr for the whitlockite structure explains the fact that hydroxyapatite formation was inhibited when strontium was introduced during the synthesis process. The stabilizing role of Mg in whitlockite has also been reported [49]. Like strontium, Mg^{2+} cation is located in the A column with a large preference for the Ca5 site in agreement with its small ionic radius.

3.4 In vitro Sr release and preliminary results on inflammation reactions in contact with Sr-HAp

The release of strontium after interaction in Sr–free culture medium (DMEM) is presented for HAp and Sr-HAp samples in Figure 7. The detection level (around 0.04 ppm) is represented by the horizontal line. Whereas no significant amount of Sr is released from undoped sample, measurable quantity of strontium ions are detected for Sr-HAp sample. The plateau concentration of ionic products (0.2 ppm) is reached after only a few days. This is an interesting amount for osteoporosis therapy: indeed it is in the same order of magnitude than the one measured *in vivo* in plasmas of animals treated with Sr-based drugs which were found to have obvious anti-osteoporotic effects [1]. The easy delivery of Sr^{2+} ions in biological conditions can be related to the observed substitution of Ca for Sr in the whitlockite phase present in Sr-doped ceramics; accordingly with the high solubility product of whitlockite compare to hydroxyapatite [37]. Indeed, some substituted strontium in the Hydroxyapatite phase is still present in the materials after this interaction time and could serve as a reservoir for future osteointegration of the implant upon bone re-modelling. Optimization of the preparation could allow to finely tune the ceramic composition (HAp/β-TCP) and thus allow a fine tuning of the delivery rate on different time scales.

3.4 Inflammatory process study: TNF-α production

In order to investigate how strontium-substituted HAp sample modulate TNF-α synthesis, monocytes cells were incubated with HAp and Sr:HAp powder for 6 hours. After 6 hours, the level of TNF-α protein was not detected in control cells. Due to the low production of TNF-α induced by the HAp powder, we have stimulated cells with LPS to investigate if the strontium had an influence on TNF-α production (Figure 8). The production of TNF-α significantly decreases for Sr-doped HAp powder (values normalized to LPS stimulated cells).Thus strontium has a positive effect on cytokines production possibly decreasing the inflammatory reactions of human monocytes in contact with HAp powder. Further work is under way to study the effect of Sr concentration and the production of other inflammatory and anti-

inflammatory cytokines. Nevertheless, this is a first promising result allowing the use of Sr-doped HAp to limit the inflammatory process during HAp implantation [50, 51].

4. Conclusions

The sol-gel process has been successfully used to prepare Sr-doped calcium phosphates. All samples are porous and exhibit phase mixtures. With respect to undoped sample, the Sr-doped sample exhibits higher proportion of β-TCP phase and significant amount of amorphous phase. As far as the substitution is concerned, Sr^{2+} ions are found in three phases, HAp, β-TCP and an amorphous phase defined as (Ca,Sr)O. These strontium ions are preferentially found in the crystalline phases (60 %) both in HAp (32%) and b-TCP (28%) but a large amount (40%) are found in the amorphous phase. From these results, it is clear that doping can be efficiently used to modulate the phase proportions and thus the solution behaviour of the material. The effective partial substitution of Sr in HAp makes this material very interesting for orthopaedic applications. The Sr-HAp cell parameters agree fairly well with the Vegard's law and Sr^{2+} ions substitute for Ca^{2+} only in the Ca2 site at low level of substitution. Sr substitution in whitlockite occurs preferentially in the Ca4 site which presents an unusually low 3-fold coordination in the pure $Ca_3(PO_4)_2$ phase.

Furthermore, the presence of Sr-containing amorphous phase and Sr-doped soluble β-TCP phase, are responsible for a partial release of Sr^{2+} ions in solution upon interaction in physiological fluids. The level of Sr^{2+} release in solution is very promising in the view of a possible anti-osteoporotic effect demonstrated by other commercial drugs. For the first time to our knowledge, a significant anti-inflammatory effect of Sr-doped HAp has been demonstrated by measuring the production of TNF-α by human monocytes in contact with the materials. Considering all these results, these materials appear to be good candidate for bone substitutes or bone tissue engineering applications combining, good bioactivity, expected anti-osteoporotic properties because of the presence of strontium and anti-inflammatory properties.

Acknowledgements

Financial support from ANR under project Nanobonefiller (PNANO 2006) is gratefully acknowledged. The authors are grateful to SNBL for the in-house beam time allocation.

References

[1] S. G. Dahl, P. Allain, P. J. Marie, Y. Mauras, G. Boivin, P. Ammann, Y. Tsouderos, P. D. Delmas and C. Christiansen, Bone, 28 (2001) 446.

[2] R. Lagier and C.-A. Baud, Pathol. Res. Pract., 199(5) (2003) 329.

[3] R. S. Lee, M. V. Kayser and S. Y. Ali, J. Anat., 208 (2006) 13.

[4] J. C. Elliot, *Structure and Chemistry of the Apatites and Other Calcium Orthophosphates*, Elsevier, Amsterdam, The Netherlands, (1994).

[5] W. E. Cabrera, I. Schrooten, M. E. De Broe and P. C. D'Haese, J. Bone Miner. Res., 14 (1999) 661.

[6] M. Cohen-Solal, Nephrol. Dial. Transplant, 17 (suppl. 2) (2002) 30.

[7] S. P. Nielsen, Bone, 35 (2004) 581.

[8] M. D. Grynpas and P. J. Marie, Bone, 11 (1990) 313.

[9] M. D. Grynpas, E. Hamilton, R. Cheung, M. Hott, P. Deloffre and P. J. Marie, Bone, 18 (1996) 253.

[10] S. Jegou Saint-Jean, C. L. Camiré, P. Nevsten, S. Hansen and M. P. Ginebra, J. Mater. Sci. Mater. Med., 16 (2005) 993.

[11] P. J. Marie, Cur. Op. Pharmacol., 5 (2005) 633.

[12] P. J. Marie, P. Ammann, G. Boivin and C. Rey, Calcif. Tissue Int., 69 (2001) 121.

[13] J. Y. Reginster, E. Seeman, M. C. De Vernejoul, S. Adami, J. Compston, C. Phenekos, J. P. Devogelaer, M. Diaz Curiel, A. Sawicki, S. Goemaere, O. H. Sorensen, D. Felsenberg and P. J. Meunier, J. Clin. Endocrinol. Metab., 90 (2005) 2816.

[14] P. J. Meunier, C. Roux, E. Seeman, S. Ortolani, J. E. Badurski, T. D. Spector, J. Cannata, A. Balogh, E.-M. Lemmel, S. Pors-Nielsen, R. Rizzoli, H. K. Genant and J.-Y. Reginster, N. Engl. J. Med., 350 (2004) 459.

[15] D. Guo, K. Xu, X. Zhao and Y. Han, Biomaterials, 26 (2005) 4073.

[16] C. T. Wong, W. W. Lu, W. K. Chang, K. M. C. Cheung, K. D. K. Luk, D. S. Lu, A. B. M. Rabie, L. F. Deng and J. C. Y. Leong, J. Biomed. Mater. Res., 68A (2004) 513.

[17] C. T. Wong, Q. Z. Cheng, W. W. Lu, J. C. Y. Leong, W. K. Chang, K. M. C. Cheung and K. D. K. Luk, J. Biomed. Mater. Res., 70A (2004) 428.

[18] K. Qiu, X. J. Xhao, C. X. Wan, C. S. Zhao and Y. M. Chen, Biomaterials, 27 (2006) 1277.

[19] C. Wu, Y. Ramaswamy, D. Kwik and H. Zreiqat, Biomaterials, 28 (2007) 3171.

[20] Y. M. Li, J. C. Y. Leong, W. W. Lu, K. D. K. Luk, K. M. C. Cheung, K. Y. Chiu and S. P. Chow, J. Biomed. Mater. Res., 52 (2000) 164.

[21] L. Leroux, M. Freche and J. L. Lacout, Key. Eng. Mater., 192-195 (2001) 235.

[22] K. Hae-Wong, K. Young-Hag, K. Young-Min, K. Young-Gu and K. Hyon-EE, J. Mater. Sci. Mater. Med., 15 (2004) 1129.

[23] F. Zhao, W. W. Lu, K. D. K. Luk, K. M. C. Cheung, C. T. Wong, J. C. Y. Leong and K. D. Yao, J. Biomed. Mater. Res., 69B (2004) 79.

[24] H. El Briak-Ben Abdeslam, B. Pauvert, A. Terol and P. Boudeville, Key. Eng. Mater., 254-256 (2004) 103.

[25] E. Landi, A. Tampieri, G. Celotti, S. Sprio, M. Sandri and G. Logroscino, Acta Biomater., 3 (2007) 961.

[26] E. Landi, S. Sprio, M. Sandri, G. Celotti and A. Tampieri, Acta Biomater., in press.

[27] D. A. Bradley, P. Muthuvelu, R. E. Ellis, E. M. Green, D. Attenburrow, R. Barrett, K. Arkill, D. B. Colridge and C. P. Winlove, Nucl. Instr. and Meth. Phys. Res., B263 (2007) 1.

[28] Z. Y. Li, W. M. Lam, C. Yang, B. Xu, G. X. Ni, S. A. Abbah, K. M. C. Cheung, K. D. K. Luk and W. W. Lu, Biomaterials, 28 (2007) 1452.

[29] W. Xue, H. L. Hosik, A. Bandyopadhyay, S. Bose, C. Ding, K. D. K. Luk, K. M. C. Cheung and W. W. Lu, Surface and Coatings technology, 201 (2007) 4685.

[30] G. X. Ni, W. W. Lu, B. Xu, K. Y. Chiu, C. Yang, Z. Y. Li, W. M. Lam and K. D. K. Luk, Biomaterials, 27 (2006) 5127.

[31] E. Jallot, J.M. Nedelec, A.S. Grimault, E. Chassot, P. Laquerriere, A. Grandjean-Laquerriere, D. Laurent-Maquin, Colloids and Surface B 42, (2005), 205.

[32] A. Grandjean-Laquerriere, P. Laquerriere, E. Jallot, J.M. Nedelec, M. Guenounou, D. Laurent-Maquin and T. Philips, Biomaterials 27, (2006), 3195-3200.

[33] J.-M. Nedelec, L. Courtheoux, E. Jallot, J. Lao, C. Kinowski, P. Laquerriere, C. Mansuy, G. Renaudin and S. Turrell, J. Sol-Gel Science and Technology (2008) Available online. DOI 10µ.1007/s10971-007-1665-0.

[34] A.P. Hammersley, S.O. Svensson, M. Hanfland, A.N. Fitch, D. Haüsermann, High Pressure Res. 14, (1996), 235.

[35] J. Rodriguez-Carvajal, PROGRA*M FullProf.2k* – version 3.20, Laboratoire Léon Brillouin (CEA-CNRS), France, 2005 (FullProf.2k manual available on http://www-llb.cea.fr/fullweb/fp2k/fp2k_divers.htm). See also J. Rodriguez-Carvajal, T. Roisnel, EPDIC-8, 23-26 May 2002, Trans. Tech. Publication Ltd, Uppsala, Sweden, Materials Science Forum 123 (2004) 443.

[36] L.M. Rodriguez-Lorenzo, J.N. Hart, K.A. Gross, J. Phys. Chem. B., 107 (2003) 8316.

[37] M. Yashima, A. Sakai, T. Kamiyama, A. Hoshikawa, J. Solid State Chem., 175 (2003) 272.

[38] R. Ganguly, V. Siruguri, I.K. Gopalakrishnan, J.V. Yakhmi, J. Phys.: Condensed Matter, 12 (2000) 1283.

[39] L. Desgranges, D. Grebille, G. Calvarin, G. Chevrier, N. Floquet, J.-C. Niepce, Acta Cryst. B, 49 (1993) 812.

[40] X. Orlhac, C. Fillet, P. Deniard, A.M. Dulac, R. Brec, J. Appl. Cryst., 34 (2001) 114.

[41] T. Ikoma, A. Yamazaki, S. Nakamura, M. Akao, J. Solid State Chem., 144 (1999) 272.

[42] M. François, G. Renaudin and O. Evrard, Acta Cryst., C54 (1998) 1214.

[43] L. Leroux and J.-L. Lacout, J. Mater. Res., 16 (2001)171.

[44] R. Lagier and C.-A. Baud, Pathol. Res. Pract., 199 (2003) 329.

[45] K. Sudarsanan, R. A. Young, Acta Cryst., B28 (1972) 3668.

[46] M. Kikuchi, A. Yamazaki, R. Otsuka, M. Akao, H. Aoki, J. Solid State Chem., **113** (1994) 373.

[47] A. Bigi, G. Falini, M. Gazzano, N. Roveri, E. Tedesco, Mat. Sci. Forum, **278** (1998) 814.

[48] N. E. Brese and M. O'Keefe, Acta Cryst., B47 (1991) 192.

[49] L. W. Schroeder, B. Dickens and W. E. Brown, J. Solid State Chem., 22 (1977) 253.

[50] A. Grandjean-Laquerriere, O. Tabary, D. Richard, J. Jacquot, P. Frayssinet, M. Guenounou, D. Laurent-Maquin, P. Laquerriere, S. Gangloff, Biomaterials, 28(2007) 400.

[51] P. Laquerriere, A. Grandjean-Laquerriere, E. Jallot, G. Balossier, P. Frayssinet, M. Guenounou, Biomaterials, 24(2003) 2739.

Table 1 : Nominal and experimental concentrations (weight %) of Ca, P, Sr in HAp and Sr HAp samples. determined by ICP-AES

	HAp	**Sr HAp**
Ca Nominal	39.88	37.02
Ca Experimental	38.46	38.79
P Nominal	18.50	18.07
P Experimental	17.21	18.42
Sr Nominal	-	4.26
Sr Experimental	-	4.23
% substitution theoretical	-	5
% substitution experimental	-	5

Table 2: Refinement results on the hydroxyapatite phase in the two HAp and Sr:HAp samples.

Phase	Atom	Site	*x*	*y*	*z*	B_{iso} (Å^2)	Occ.[b]
$Ca_5(PO_4)_3(OH)$	Ca1	4*f*	1/3	2/3	0.0013(2)	0.29(2)	1(-)
$P6_3/m$, $Z = 2$	Ca2	6*h*	0.2462(1)	0.9926(1)	¼	$= B_{(Ca1)}$	1(-)
$a = 9.4239(1)$ Å	P1	6*h*	0.3988(2)	0.3691(2)	¼	0.38(3)	1(-)
$c = 6.8841(1)$ Å	O1	6*h*	0.3260(3)	0.4830(3)	¼	0.12(3)	1(-)
R_{Bragg} [a] = 0.026; 0.013	O2	6*h*	0.5875(3)	0.4653(3)	¼	$= B_{(O1)}$	1(-)
*R*p [a] = 0.021; 0.018	O3	12*i*	0.3407(2)	0.2559(2)	0.0704(2)	$= B_{(O1)}$	1(-)
*R*wp [a] = 0.029; 0.027	O4	4*e*	0	0	0.2030(9)	$= B_{(O1)}$	½(-)
	H4	4*e*	0	0	0.073(3)	$= 1.2xB_{(O1)}$	½(-)
$Ca_{4.88(1)}Sr_{0.12(1)}(PO_4)_3(OH)$	Ca1	4*f*	1/3	2/3	0.0036(6)	0.43(4)	1(-)
$P6_3/m$, $Z = 2$	Ca2	6*h*	0.2469(2)	0.9932(3)	¼	$= B_{(Ca1)}$	0.964(2)
$a = 9.4305(3)$ Å	Sr2	6*h*	$= x_{(Ca2)}$	$= y_{(Ca2)}$	$= z_{(Ca2)}$	$= B_{(Ca1)}$	$= 1\text{-}Occ_{(Ca2)}$
$c = 6.8887(2)$ Å	P1	6*h*	0.4016(4)	0.3694(4)	¼	0.27(7)	1(-)
R_{Bragg} [a] = 0.028; 0.017	O1	6*h*	0.3289(7)	0.4829(7)	¼	0.54(8)	1(-)
*R*p [a] = 0.012; 0.018	O2	6*h*	0.5849(7)	0.4627(7)	¼	$= B_{(O1)}$	1(-)
*R*wp [a] = 0.016; 0.026	O3	12*i*	0.3416(4)	0.2563(5)	0.0704(5)	$= B_{(O1)}$	1(-)
	O4	4*e*	0	0	0.191(1)	$= B_{(O1)}$	½(-)
	H4	4*e*	0	0	0.057(3)	$= 1.2xB_{(O1)}$	½(-)

[a] two values represent the measurements performed at 150 and 350 mm respectively, [b] site occupancy factor.

Table 3: Refinement results on the withlockite phase in the Sr:HAp sample.

Phase	Atom	Site	x	y	z	B_{iso} (Å^2)	Occ.[b]
$Ca_{2.87(6)}Sr_{0.13(6)}(PO_4)_2$	Ca1	18*b*	0.728(1)	0.861(2)	0.1700(7)	0.30(9)	1(-)
*R*3*c*, *Z* = 21	Ca2	18*b*	0.620(1)	0.816(2)	-0.0311(7)	= $B_{(Ca1)}$	1(-)
a = 10.4471(4) Å	Ca3	18*b*	0.7320(9)	0.843(1)	0.0634(7)	= $B_{(Ca1)}$	0.90(2)
c = 37.391(2) Å	Sr3	18*b*	= $x_{(Ca3)}$	= $y_{(Ca3)}$	= $z_{(Ca3)}$	= $B_{(Ca1)}$	= 1-$Occ_{(Ca3)}$
R_{Bragg} [a] = 0.041; 0.027	Ca4	6*a*	0	0	-0.0822(8)	= $B_{(Ca1)}$	0.25(2)
*R*p [a] = 0.012; 0.018	Sr4	6*a*	= $x_{(Ca4)}$	= $y_{(Ca4)}$	= $z_{(Ca4)}$	= $B_{(Ca1)}$	= ½-$Occ_{(Ca4)}$
*R*wp [a] = 0.016; 0.026	Ca5	6*a*	0	0	0.7329(8)	= $B_{(Ca1)}$	0.96(2)
	Sr5	6*a*	= $x_{(Ca5)}$	= $y_{(Ca5)}$	= $z_{(Ca5)}$	= $B_{(Ca1)}$	= 1-$Occ_{(Ca5)}$
	P1	6*a*	0	0	0(-)	1.8(2)	1(-)
	P2	18*b*	0.683(1)	0.862(3)	0.8656(8)	= $B_{(P1)}$	1(-)
	P3	18*b*	0.651(2)	0.848(2)	0.7651(7)	= $B_{(P1)}$	1(-)
	O1	18*b*	0.714(3)	-0.105(4)	-0.088(1)	1.0(1)	1(-)
	O2	18*b*	0.758(4)	0.766(4)	0.851(1)	= $B_{(O1)}$	1(-)
	O3	18*b*	0.743(5)	0.006(4)	0.850(1)	= $B_{(O1)}$	1(-)
	O4	18*b*	0.507(3)	0.756(5)	0.861(1)	= $B_{(O1)}$	1(-)
	O5	18*b*	0.603(4)	-0.043(4)	0.775(1)	= $B_{(O1)}$	1(-)
	O6	18*b*	0.567(3)	0.697(5)	0.783(1)	= $B_{(O1)}$	1(-)
	O7	18*b*	0.117(3)	0.919(4)	0.777(1)	= $B_{(O1)}$	1(-)
	O8	18*b*	0.630(3)	0.835(3)	0.729(1)	= $B_{(O1)}$	1(-)
	O9	18*b*	0.024(3)	0.871(3)	-0.019(1)	= $B_{(O1)}$	1(-)
	O10	6*a*	0	0	0.045(1)	= $B_{(O1)}$	1(-)

[a] two values represent the measurements performed at 150 and 350 mm respectively, [b] site occupancy factor.

Table 4: Results of the quantitative phase analyses using the Rietveld method. An amorphous (Ca,Sr)O amount was estimated assuming the refined values for the crystalline phases and the synthesis conditions: (Ca+Sr)/PO_4= 1.67 with 5 at % of Sr.

Sample		Apatite		Sr:apatite	
Synthesis	(Ca+Sr)/PO_4	**1.67**		**1.67**	
	Sr amount	**0 %**		**5.0 %**	
Refined	*Phase*	*Formula*	*Wt %*	*Formula*	*Wt %*
	Apatite	$Ca_5(PO_4)_3(OH)$	92.8(6)	$Ca_{4.88(1)}Sr_{0.12(1)}(PO_4)_3(OH)$	66.5(6)
	whitlockite	$Ca_3(PO_4)_2$	7.0(3)	$Ca_{2.87(6)}Sr_{0.13(6)}(PO_4)_2$	32.6(5)
	lime	CaO	0.2(1)	CaO	0.5(1)
	portlandite	-	-	$Ca(OH)_2$	0.4(1)
	(Ca+Sr)/PO_4	**1.66(2)**		**1.63(3)**	
	Sr amount	**0(-) %**		**2.86(4) %**	
Estimated assuming the used synthesis ratios	*Phase*			*Formula*	*Wt %*
	apatite			$Ca_{4.88}Sr_{0.12}(PO_4)_3(OH)$	65.0
	whitlockite			$Ca_{2.87}Sr_{0.13}(PO_4)_2$	31.9
	lime			CaO	0.5
	portlandite			$Ca(OH)_2$	0.4
	amorphous[a]			$(Ca,Sr)O_{amorph.}$	2.2
	(Ca+Sr)/PO_4			**1.67(-)**	
	Sr amount			**5.0(-) %**	

[a] refers to 'an amorphous (Ca,Sr)O' in the text.

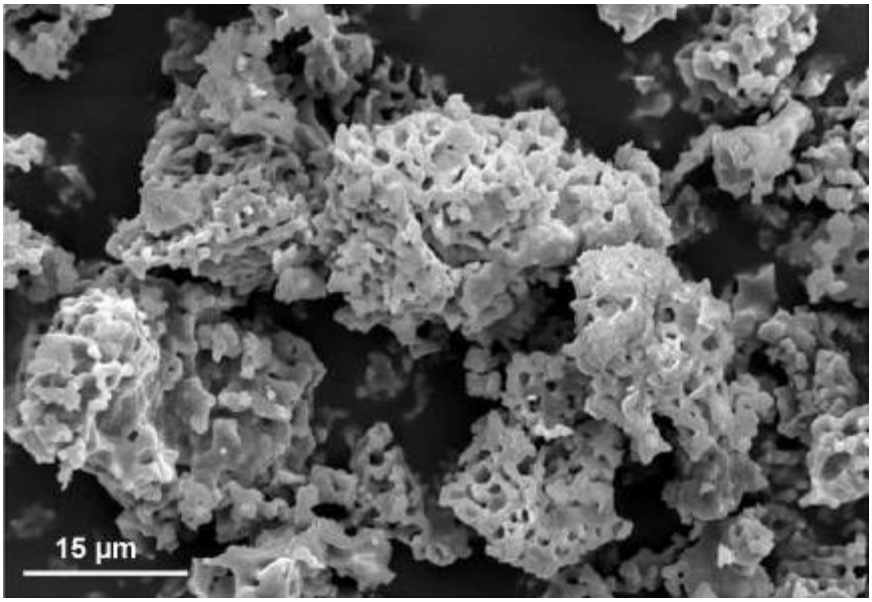

Figure 1: Representative SEM image of sol-gel derived HAp samples.

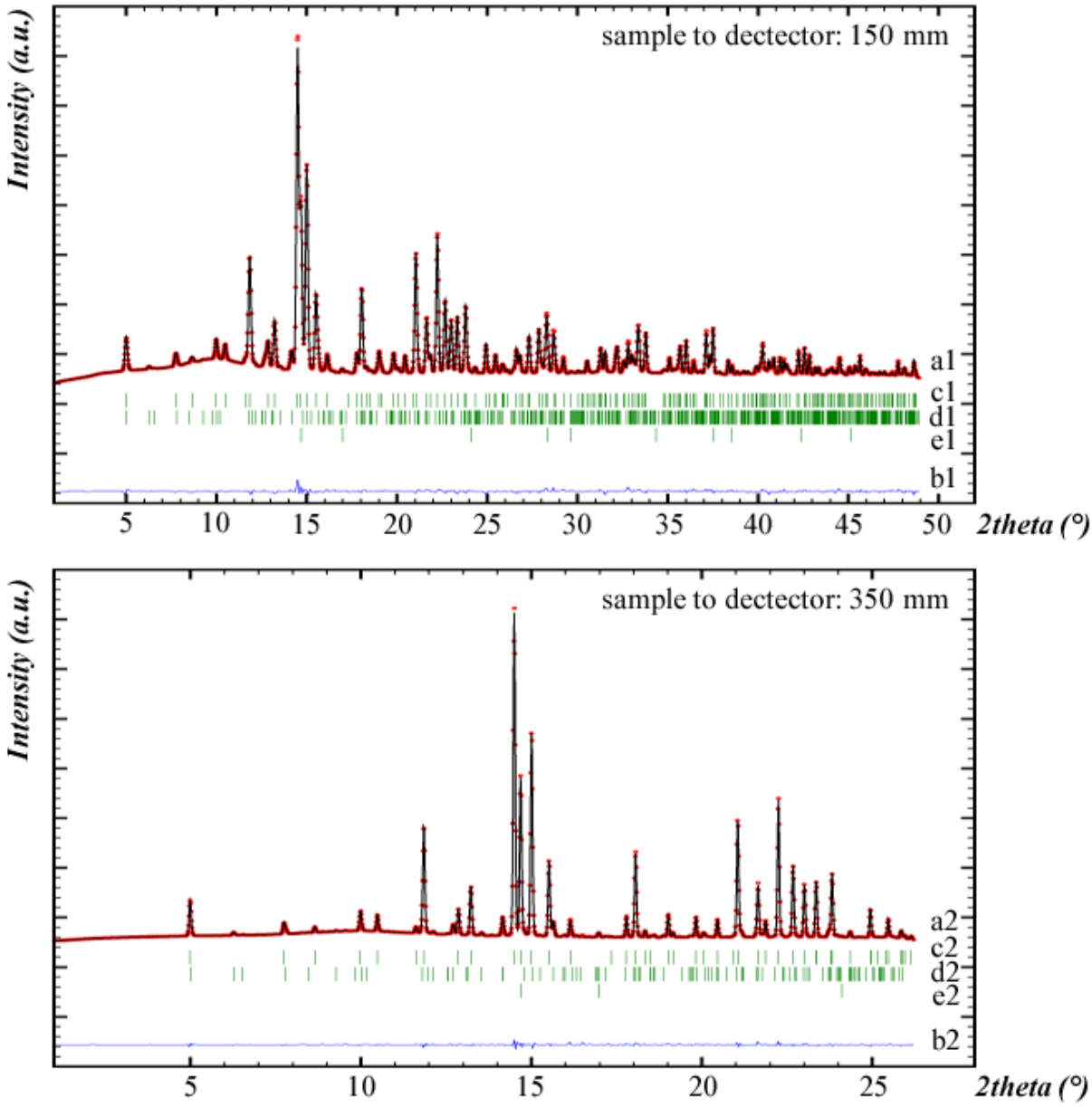

Figure 2: Powder patterns from the Joint Rietveld on the HAp sample. Two sample-to-detector distances represent top (150 mm) and bottom (350 mm) plots. The data were measured at SNBL, ESRF with MAR345 Image Plate detector and λ = 0.710130 Å. Observed (a1 and a2; red dots), calculated (a1 and a2; black lines) and difference (b1 and b2; blue lines) powder diffraction patterns are presented. Bragg positions are indicated by green vertical bars for hydroxyapatite (c1 and c2), whitlockite (d1 and d2) and lime (e1 and e2).

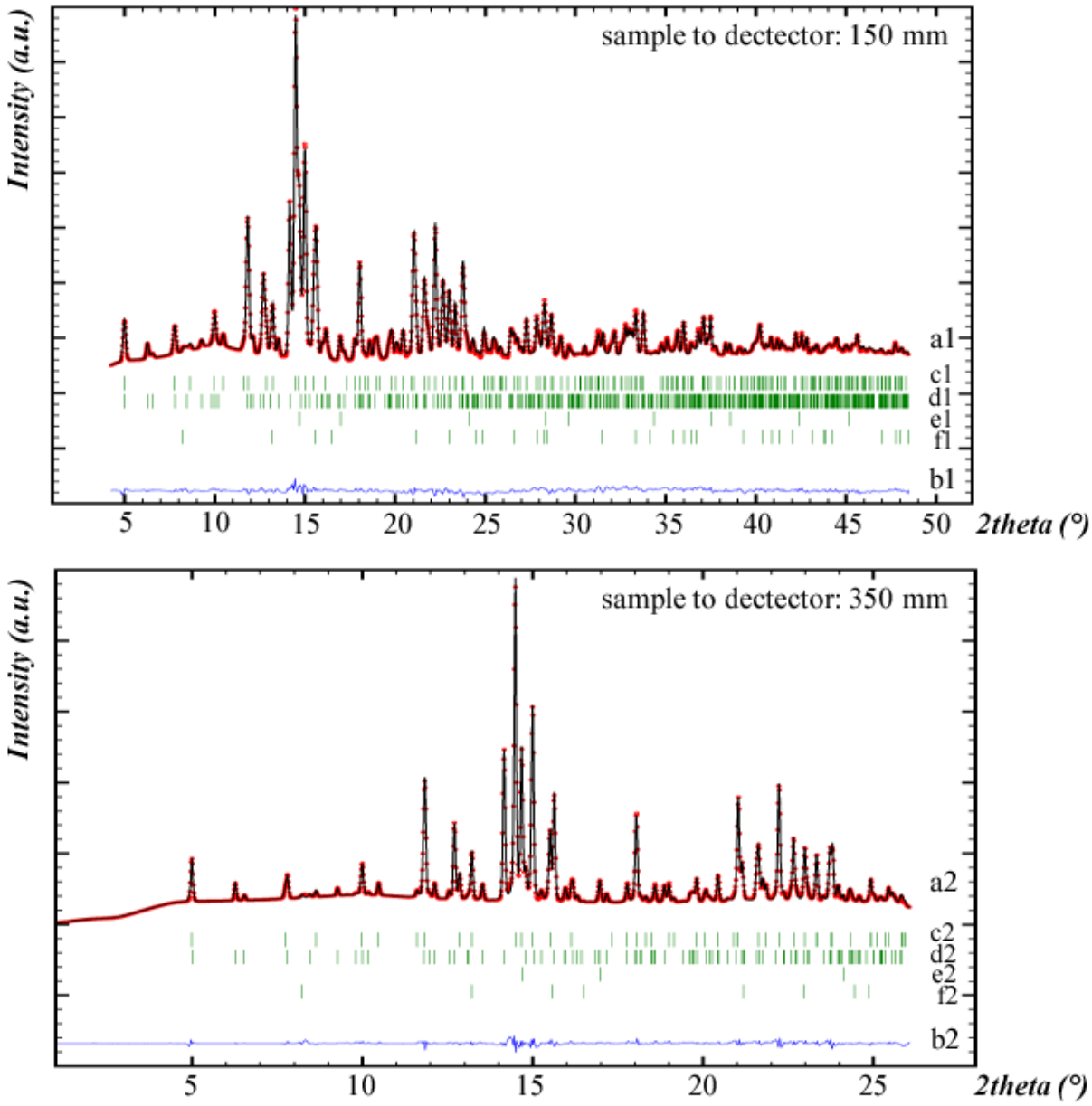

Figure 3: Powder patterns from the joint Rietveld on the Sr:HAp sample. Two sample-to-detector distances represent top (150 mm) and bottom (350 mm) plots. The data were collected at SNBL, ESRF with MAR345 Image Plate detector and $\lambda = 0.710130$ Å. Observed (a1 and a2; red dots), calculated (a1 and a2; black lines) and difference (b1 and b2; blue lines) powder diffraction patterns are presented. Bragg positions are indicated by green vertical bars for hydroxyapatite (c1 and c2), whitlockite (d1 and d2), lime (e1 and e2) and portlandite (f1 and f2).

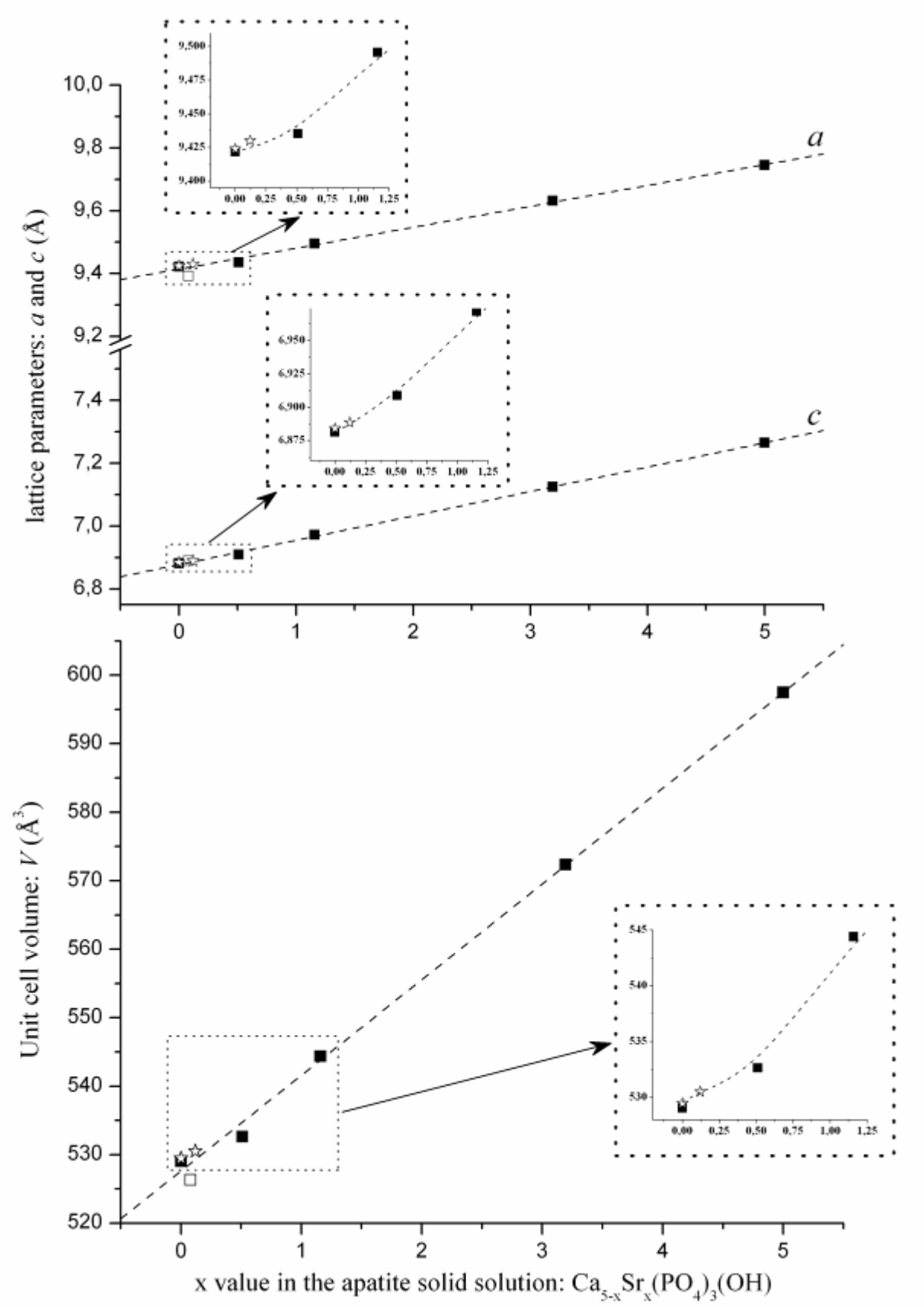

Figure 4: Lattice parameters (top) and unit cell volume (bottom) as a function of the x value for the solid solution $Ca_{10-x}Sr_x(PO_4)_6(OH)_2$. Details on the Ca-rich side are shown in the insets.

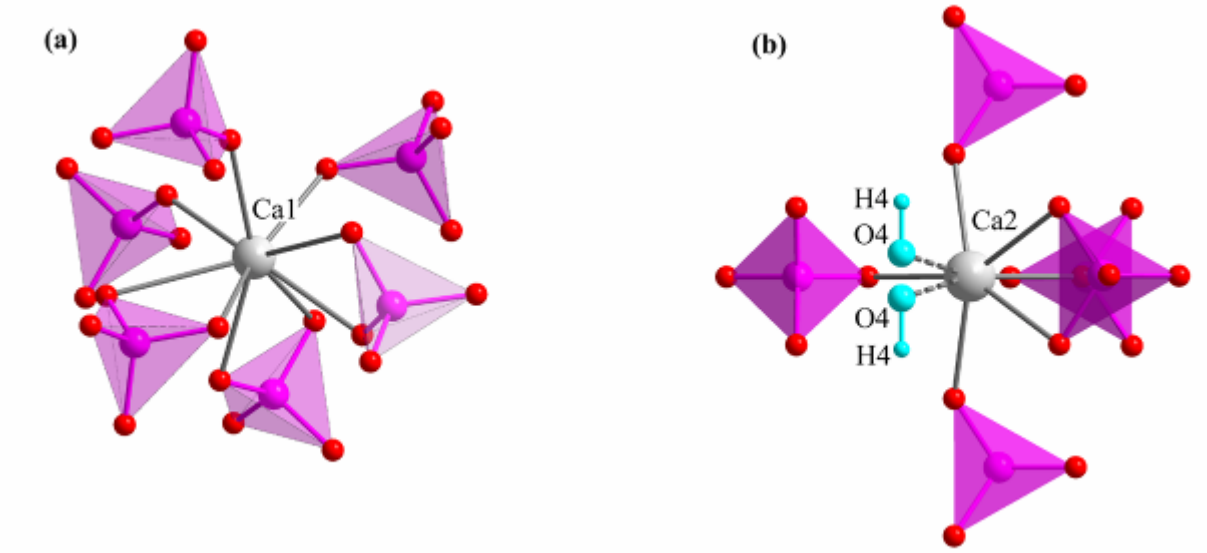

Figure 5: Calcium environments of Ca1 site (a) and Ca2 site (b) in the hydroxyapatite structure. Grey, pink, red and blue balls represent respectively calcium, phosphorus and oxygen atoms and hydroxyl groups. Phosphate tetrahedra are coloured in pink.

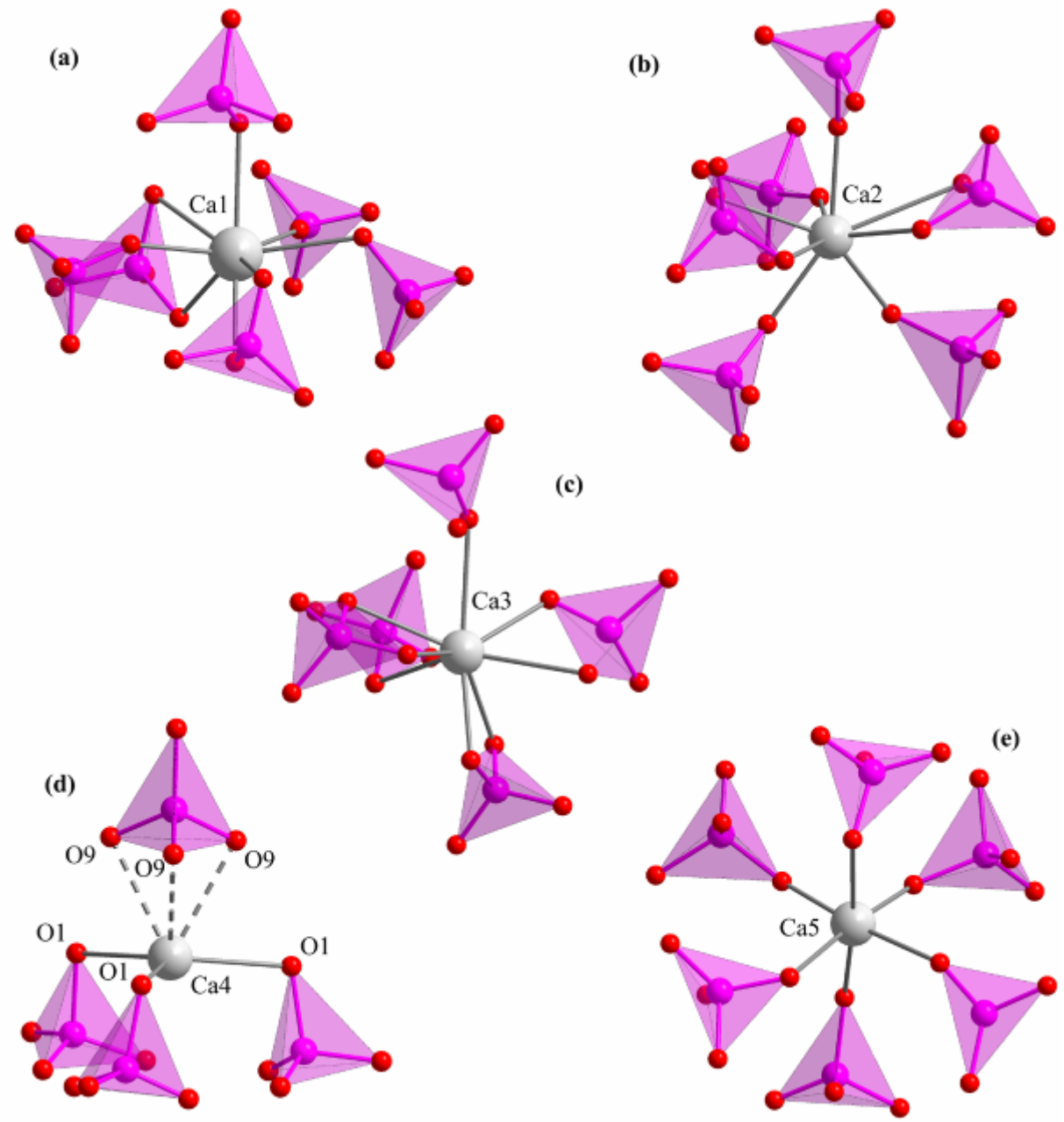

Figure 6: Calcium environments of Ca1 site (a), Ca2 site (b), Ca3 site (c), Ca4 site (d) and Ca5 site (e) in the whitlockite structure. Grey, pink and red balls represent respectively calcium, phosphorus and oxygen atoms. Phosphate tetrahedra are coloured in pink.

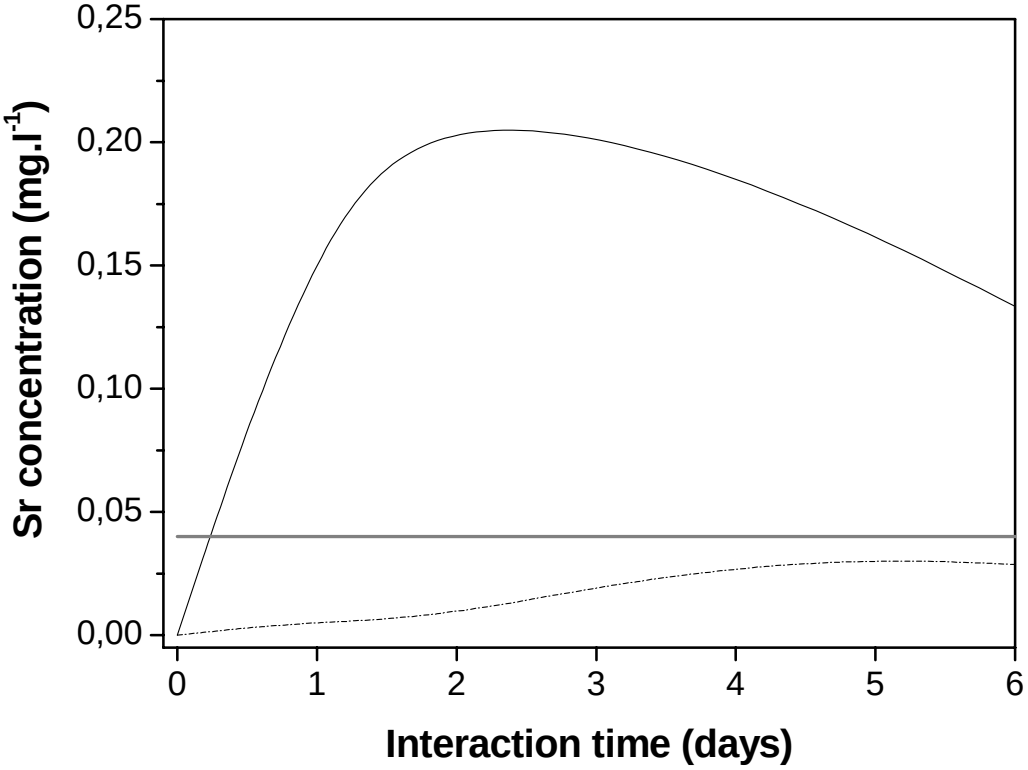

Figure 7 : Release of strontium ions as a function of interaction time for Sr-HAp (solid line) and HAp (dotted line) samples. The horizontal grey line represents the detection level.

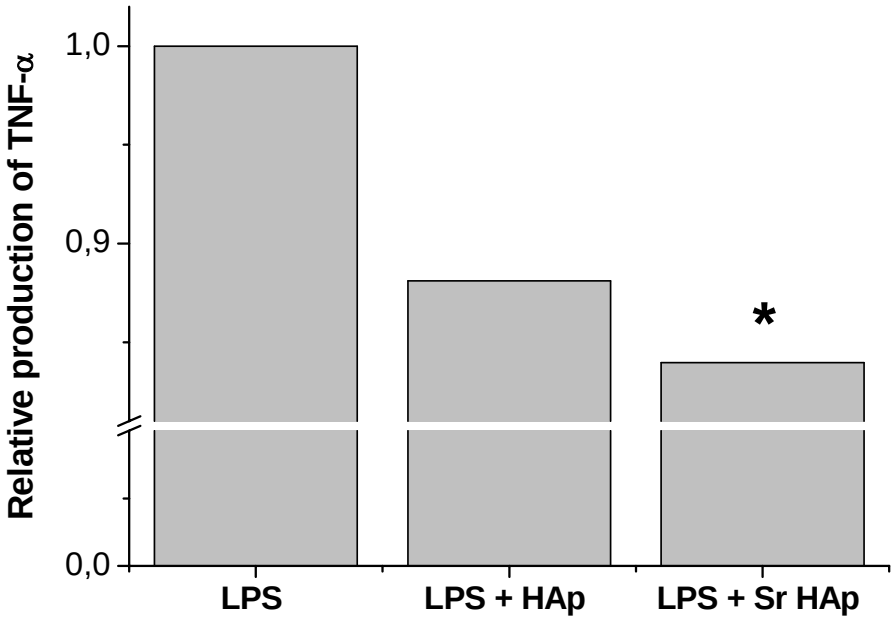

Figure 8 : Tumor Necrosis Factor (TNF-α) production by human monocytes cultured for 6 hours with LipoPolySaccharide (LPS) without material and in contact with HAp and Sr-HAp samples (* means $p<0.05$).